HHS Public Access

Author manuscript

ACS Nano. Author manuscript; available in PMC 2016 April 20.

Published in final edited form as:

ACS Nano. 2016 March 22; 10(3): 3486–3495. doi:10.1021/acsnano.5b07671.

A Photosensitizer-Loaded DNA Origami Nanosystem for Photodynamic Therapy

Xiaoxi Zhuang[⊥,†], **Xiaowei Ma**[*,⊥,†], **Xiangdong Xue**[†], **Qiao Jiang**[‡], **Linlin Song**[‡], **Luru Dai**[‡], **Chunqiu Zhang**[†], **Shubin Jin**[†], **Keni Yang**[†], **Baoquan Ding**[‡], **Paul C. Wang**[§,‖], and **Xing-Jie Liang**[*,†]

[†]Laboratory of Controllable Nanopharmaceuticals, CAS Key Laboratory for Biomedical Effects of Nanomaterials and Nanosafety, National Center for Nanoscience and Technology, Beijing 100190, China

[‡]CAS Key Laboratory of Nanosystem and Hierarchical Fabrication, National Center for Nanoscience and Technology, Beijing 100190, China

[§]Fu Jen Catholic University, Taipei 24205, Taiwan

[‖]Laboratory of Molecular Imaging, Department of Radiology, Howard University, Washington, DC 20060, United States

Abstract

Photodynamic therapy (PDT) offers an alternative for cancer treatment by using ultraviolet or visible light in the presence of a photosensitizer and molecular oxygen, which can produce highly reactive oxygen species that ultimately leading to the ablation of tumor cells by multifactorial mechanisms. However, this technique is limited by the penetration depth of incident light, the hypoxic environment of solid tumors, and the vulnerability of photobleaching reduces the efficiency of many imaging agents. In this work, we reported a cellular level dual-functional imaging and PDT nanosystem BMEPC-loaded DNA origami for photodynamic therapy with high efficiency and stable photoreactive property. The carbazole derivative BMEPC is a one- and two-photon imaging agent and photosensitizer with large two-photon absorption cross section, which can be fully excited by near-infrared light, and is also capable of destroying targets under anaerobic condition by generating reactive intermediates of Type I photodynamic reactions. However, the application of BMEPC was restricted by its poor solubility in aqueous environment and its aggregation caused quenching. We observed BMEPC-loaded DNA origami effectively reduced the photobleaching of BMEPC within cells. Upon binding to DNA origami, the intramolecular rotation of BMEPC became proper restricted, which intensify fluorescence emission and radicals production when being excited. After the BMEPC-loaded DNA origami are

[*]**Corresponding Authors**: maxw@nanoctr.cn. liangxj@nanoctr.cn.

[⊥]**Author Contributions**

These authors contributed equally to this work.

Supporting Information

The Supporting Information is available free of charge on the ACS Publications website at DOI: 10.1021/acsnano.5b07671. Additional figures including AFM images, UV–vis absorption spectra, CLSM images, and so on. (PDF)

Notes

The authors declare no competing financial interest.

taken up by tumor cells, upon irradiation, BMEPC could generate free radicals and be released due to DNA photocleavage as well as the following partially degradation. Apoptosis was then induced by the generation of free radicals. This functional nanosystem provides an insight into the design of photosensitizer-loaded DNA origami for effective intracellular imaging and photodynamic therapy.

Graphical abstract

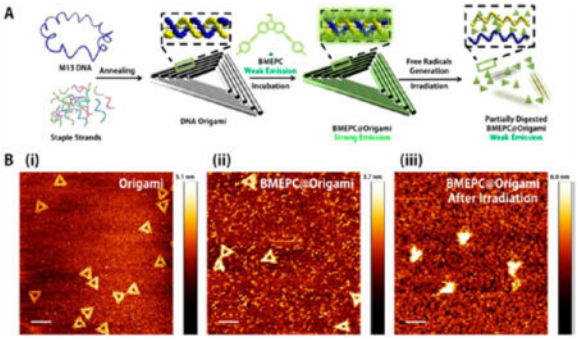

Keywords

carbazole derivative photosensitizer; DNA origami; intracellular imaging; photodynamic therapy; dual-functionality

Malignant cancer accounted for millions of deaths worldwide every year, and the number is continuously rising. However, clinically available treatment options such as surgery, chemotherapy, and radiotherapy are limited due to high recurrence rate, systemic side effects, and cumulative radiation dose, respectively.[1] Photodynamic therapy (PDT) offers great promise for cancer treatment by using ultraviolet (UV) or visible radiation, especially lasers, in the presence of a photosensitizer (PS) and molecular oxygen, which can produce highly reactive oxygen species (ROS) that ultimately leading to tumor cell ablation.[2–9] ROS can oxidize lipids, amino acids and proteins, inducing irreversible damage to vital organelles and plasma membrane. Then, induced cell death can be accomplished by cell apoptosis as well as necrosis and autophagy, which does not depend on the phase of the cell cycle.[10,11] Over the last semicentury, PDT has proven to be effective in many kinds of cancers.[12–15] Compared with the aforementioned three treatment modalities, PDT has the merits of minimal invasion, low poison, precise operation, and nondrug resistance.[5,16–19] Also, it is suitable for being used as an adjuvant for surgery.[20–22]

Although PDT is widely spread and accepted, it has not been applied as a first-line oncological treatment due to certain limitations. First, the hypoxic environment of solid tumors hinders the efficiency of type II photodynamic reactions.[23–25] However, type I photodynamic reactions can generate ROS by electron transfer and hydrogen abstraction processes, and do not rely on oxygen molecules.[26,27] Besides, conventional one-photon PSs have the drawback of UV or visible light excitation, which limit the penetration depth,[28] whereas two-photon PS can simultaneously absorb two less energetic photons into the excited state. In addition, common organic PSs are less photostable and may be subject to

photoinduced degradation,[29] especially under two-photon excitation, which are not suitable for long-term PDT application. So, it is necessary to reduce the irradiation time or intensity to achieve more effective PDT.

Novel PS 3, 6-bis[2-(1-methylpyridinium) ethynyl]-9-pentyl-carbazole diiodide (BMEPC) is a carbazole derivative (chemical structure is shown in Figure S1A) of low molecular weight (M_W = 723), which is capable of functioning *via* Type I and Type II photodynamic reactions generating both free radicals and singlet oxygen ($^1O_2$)[30] (normalized UV–vis absorption and fluorescence emission spectrum in ddH_2O is shown in Figure S1B). In solid tumor tissues, there is little molecular oxygen to be utilized. Type I photodynamic reaction products, the reactive intermediates from electron transfer and hydrogen abstraction, will fit the hypoxic cellular areas well.[31,32] Besides, BMEPC has two-photon absorption (TPA) ability with a large TPA cross section (522 GM at 760 nm), which can be fully excited by near-infrared (NIR) light.[30] The excitation in the NIR region (spectral window: 700–1100 nm) avoids tissue absorbing and makes it possible to reach deep tissues *in vivo*.[33]

According to the previous work, BMEPC has low solubility and quantum yield in aqueous environment until binding toward DNA macromolecules by intercalating into the base pairs.[30] When binding to DNA double helix, BMEPC shows much higher fluorescence emission, which perhaps arises from the spatial confinement of free rotated aromatic groups. Considering BMEPC is a positively charged molecule which has a perfect binding affinity toward negatively charged DNA double helix, and self-assembled DNA nanostructures exhibit little cytotoxicity or immunogenicity, along with relative stability in aqueous solution as well as cellular environment,[34–37] we would like to perform the irradiation process with less time or intensity, making use of the restriction of DNA nanostructures.

Comparatively, DNA origami has a greater potential to deliver BMEPC molecules than any other DNA nanostructures such as aptamers, because the additional layers of tightly packed double helices supply many more and denser intercalation sites.[38] The tightly packed double helices avoid the combination of DNA hydrolases in cellular environment, and the high density of BMEPC molecules means an increased fluorescence emission and photodynamic efficiency.

In this study, we developed a BMEPC restricted and delivered nanosystem using two-dimensional triangular-shaped DNA origami as the nanocarrier. When incubated with regular human breast adenocarcinoma cancer cells MCF-7, BMEPC-loaded DNA origami complex would be internalized by the cells. After being taken into the cells, the complex could play the roles of both imaging and photosensitizing agents inside MCF-7 cells. Also, ROS free radicals generated upon one- or two-photon irradiation will finally lead to cell ablation.

RESULTS AND DISCUSSION

First, we performed a solvent-dependent aggregation caused fluorescence variation experiment to study the fluorescence-aggregates correlation of BMEPC molecules. We dissolved BMEPC into its good solvent (dimethyl sulfoxide, DMSO) and gradually

increased the poor solvent (ddH_2O) proportions to obtain the BMEPC molecules in different aggregation state. According to the fluorescence variations in Figure S2, the intramolecular rotations of BMEPC molecules would consume the excitation energy in dispersed state and, thus, showed rather low fluorescence emission but was enhanced owing to the restricted intramolecular rotation (RIR) with the percentage of ddH_2O increasing at the beginning. However, when it was above 30%, the fluorescence decreased rapidly due to the aggregation-caused quenching (ACQ). The fluorescence variations in different fractions of DMSO/ddH_2O demonstrated that only under proper aggregation or intramolecular restriction state could BMEPC molecules show good fluorescent imaging behaviors, whereas under the excessive aggregation state, they will go in the opposite direction. Therefore, we can see carrier-free BMEPC in pure ddH_2O showed nonuniformity in size (Figure 1A) and extremely low fluorescence emission (Figure 1B and C).

Then, the triangular-shaped DNA origami self-assembled with M13 phage DNA scaffold and staple strands (Scheme 1). Observation of the morphology of the synthesized DNA origami by atomic force microscopy (AFM) (Figure S3) showed a neat triangular-shape with a uniform size. Each outer edge of the triangle was about 115 nm, and the height appeared 2 nm or so, which were in line with the literature reported.[39] We hoped they could offer BMEPC molecules a proper restricted space.

After loading BMEPC at room temperature, the origami appeared a little larger in size, but remained its morphology (Figure 1E). In order to make full use of the carrier, we estimated the maximum loading capacity of BMEPC on one DNA origami. We mixed DNA origami and BMEPC with different molar ratios to form the complexes and evaluated their UV–vis absorption and fluorescence emission variations. As shown in Figure S4A and S4B, upon binding to DNA origami, the maximum absorption of BMEPC decreased slightly and bathochromically shifted 10–18 nm. The fluorescence emission spectra also exhibited a corresponding bathochromic shift (Figure 1C and G). The wavelength shifts meant that the structure of BMEPC might have changed when it bound with DNA origami.[40] At the same time, the origami-bound BMEPC showed obvious fluorescence enhancement compared with carrier-free BMEPC (Figure 1B and F). When the ratio of BMEPC was 5000, the fluorescence intensity of carrier-free BMEPC was less than 100 (Figure 1C) and would dramatically increase to over 700 binding with DNA origami (Figure 1G). This evidence also suggested that BMEPC molecules were successfully loaded. Comparing the fluorescence enhancement among different molar ratio mixes, we could find that with more BMEPC added into DNA origami aqueous solutions, the fluorescence intensity of the complex was enhanced accordingly with a linear increment of the BMEPC ratios up to 20 000 (Figure 1D and 1H). It is likely that one triangular-shaped DNA origami could load about 20 000 BMEPC molecules at most. If we kept adding, the extra part of BMEPC may aggregate on the surface of DNA origami, which limited the follow-up fluorescence enhancement and bathochromic shift. In Figure 1I, we could also make out that when the ratio of BMEPC was 20 000, the fluorescence emission showed the most significant enhancement, so we chose this ratio in the following experiments.

Theoretically, when BMEPC photosensitizers were loaded onto the DNA origami and the intramolecular rotation was physically restricted, their excitation energy would be partially

dissipated in form of fluorescence, and the PDT effect would also take place. So we conducted light irradiation on BMEPC-loaded DNA origami with a 365 nm UV lamp. As shown in Figure 2B, broken triangles were clearly visible, which indicated the origami structure was partially damaged. It means that BMEPC was successfully loaded and showed excellent DNA destruction ability when exited.

To examine the photodegradation ability of BMEPC-loaded DNA origami nanosystem, we conducted different molar ratios of the complex with agarose gel electrophoresis (AGE) analysis to evaluate the DNA degradation phenomenon. Unloaded DNA origami and carrier-free BMEPC were also employed here as control. AGE results in Figure 2C showed that under the same lighting conditions, the intensity of the AGE bands were getting shallower according to the increasing BMEPC ratios in the initial mixes. Unloaded DNA origami samples showed no shallow bands changes, and carrier-free BMEPC samples were with no bands before and after irradiation. These results indicated that the lighting condition we used here did not damage the unloaded DNA nanostructure and with the increase of BMEPC molar ratio, better PDT efficiency presented, which was in line with the fluorescence emission.

To investigate the influence of irradiation time on photodegradation ability, the BMEPC-loaded DNA origami complex was exposed to a 365 nm UV lamp under different irradiation time. As shown in Figure 2D, the intensity of the AGE bands was fading gradually, corresponding to the prolongation of irradiation time. Meanwhile, the fluorescence intensity of BMEPC-loaded DNA origami complex also decreased (Figure 2E). The decreasing of BMEPC-loaded DNA origami fluorescence was brought about by both of the release of BMEPC molecules from degradative DNA origami structure and photobleaching. The photobleaching phenomenon demonstrated that free radicals were successfully generated and the fading behaviors of AGE bands illustrated the DNA origami could be effectively destroyed by free radicals and therefore BMEPC was released from the carriers.

To confirm whether the negatively charged complex could be internalized by cells, vertical section scanning was implemented along the z axis after 12 h incubation with MCF-7 cells. Micrographs were taken while moving the focal plane with incremental steps from the dish bottom to the top of the cells. From the confocal laser scanning microscopy (CLSM) images (Figure S5), BMEPC-loaded DNA origami complex was effectively taken up by MCF-7 cells, and showed clearly fluorescent imaging feature at subcellular level, which indicated that our nanosystem seamlessly integrate the intracellular imaging and PDT functionalities in a single complex.

Before being used for cell experiments, biocompatibility of the photosensitizers and biosafety of the light were evaluated. By MTT assay, cell viabilities after incubated with different concentrations of carrier-free BMEPC were tested using MCF-7 cells (Figure 3A), and the results indicated that BMEPC showed good biocompatibility under low concentrations. Hence, we chose 20 μM BMEPC to conduct the cell experiments, as the cell viability was more than 95% under this concentration. Irradiation alone without other treatment within 30 min showed very slight influence on the cells (Figure 3B). We then disposed the cells using carrier-free BMEPC and BMEPC-loaded DNA origami respectively,

and both of them showed good cell killing ability after irradiation for 30 min. However, the 50% inhibitive time of irradiation had significant difference (Figure 3C, $p < 0.001$), indicating that BMEPC-loaded DNA origami had better PDT efficacy than carrier-free BMEPC.

To confirm whether cell apoptosis was triggered after irradiation, apoptosis fluorescence staining was performed with Annexin V/Dead Cell Apoptosis Kit. The apoptosis was directly observed by CLSM (Figure 3D). Before irradiation, the cells stayed in very healthy state. After being irradiated for 600 s, the phosphatidylserine exposed on the internal cell surfaces was specifically stained by Annexin V, suggesting that most cells enter the apoptosis process. In the bright field, the cell morphology was disturbed, and we could observe obvious membrane blebbing occurrence. Therefore, in the following experiments, we used membrane blebbing as visual identification to assess whether the cells undergo apoptosis.

After evaluating the cell viability and apoptosis, we conducted CLSM imaging and irradiating experiment to prove the intracellular imaging and PDT functionalities of our materials. The results of one-photon CLSM images were shown in Figure 4. For the control cells, no membrane blebbing was observed with continuous laser irradiation (Figure 4A). With carrier-free BMEPC treatment and irradiated under the laser, the cells lived in healthy state in the first 300 s, but undergo apoptosis from 480 s irradiation, as obvious membrane blebbing could be observed (Figure 4B). And in BMEPC-loaded DNA origami treatment group (Figure 4C), all cells started apoptosis from 300 s irradiation.

Moreover, we noticed that without the protection of DNA origami, the carrier-free BMEPC displayed worse antiphotobleaching ability (Figure 5). We suspected that the rigid structure of DNA origami provided an optimal restricted degree avoiding ROS generating too fast to release BMEPC rapidly. The ROS staining experiments confirm the speculation. With carrier-free BMEPC treatment, the brightest ROS fluorescence emission appeared after irradiated for 300 s, wherea the BMEPC-loaded DNA origami treatment group showed brightest emission after irradiated for 660 s (Figure 6). We speculated that longer virtual function time of BMEPC under the protection of DNA origami would be responsible for the higher PDT efficacy of BMEPC-loaded DNA origami. Nevertheless, further studies are still underway to investigate the detailed molecular mechanisms of how BMEPC works.

PDT treatments require excellent tissue penetration abilities because most cancer tissues were hidden under the skin. Photosensitizers with two-photon absorption ability can be excited by NIR light, and NIR light provide excellent tissue penetration ability. The BMEPC molecule used in our study exhibited unique two-photon excitation behavior. Therefore, we treated MCF-7 cells with carrier-free BMEPC or BMEPC-loaded DNA origami, respectively, under 800 nm two-photon irradiation. Similarly, we could see the untreated cells showed no evidence of apoptosis in 180 s in control experiment (Figure S6A), indicating that the two-photon laser we used here did not hurt the cells. Then the carrier-free BMEPC treated group showed little membrane blebbing occurrence within 180 s, whereas the fluorescence emission nearly vanished (Figure S6B). On the contrary, in BMEPC-loaded DNA origami treated group, the cells undergo apoptosis after 180 s irradiation, and at that

time we could still see some fluorescence emission (Figure S6C). By comparing the one- and two-photon induced CLSM images, we could come to the same conclusion that the BMEPC-loaded DNA origami are excellent candidate for PDT treatments.

Although DNA origami has limited targeting functionality, it is very convenient to be modified by DNA aptamers through base-pairing interactions. DNA aptamers have been proved to have superior cell selectivity by binding to specific targets in cells or on cell surface. Appropriate aptamer-tagged DNA origami can selectively and effectively target the cancer cells.[41–43]

CONCLUSION

A self-assembled photosensitizers-loaded DNA origami nanosystem serving as a novel dual-functional theranostic agent was reported in this work. Our results displayed BMEPC-loaded DNA origami complex showed better abilities than carrier-free BMEPC in imaging and photodynamic aspects, which demonstrated a promising candidate for intracellular imaging and cancer therapy. Carrier-free BMEPC has low quantum yield in aqueous solution due to ACQ and displayed weak antiphotobleaching ability within cells. After binding to DNA origami, the intramolecular rotation of BMEPC became properly restricted, and more excitation energy is dissipated in form of fluorescence emission and free radicals production. After irradiation, DNA origami nanostructure effectively protected BMEPC molecules from photobleaching, and under the protection, BMEPC could emit visible fluorescence for a longer time, then the free radicals induced cell apoptosis. This platform should also be applicable to other photosensitizers, making it widely applied. In conclusion, this work provides new insights into novel multifunctional DNA origami-based nanostructures for photosensitizer delivery in photodynamic cancer therapy.

MATERIALS AND METHODS

Materials

Yellow powdered 3,6-bis[2-(1-methylpyridinium)ethynyl]-9-pentyl-carbazole diiodide (BMEPC) was generously provided by Dr. Yongchao Zheng and stored under protection from light at 4 °C. DNA oligonucleotides were obtained from Integrated DNA Technologies or Invitrogen China. The origami staple strands were stored in 96-well plates with concentrations normalized to 100 μM and used without further purification. The concentration of each strand was estimated by measuring the UV absorbance at 260 nm. M13 phage DNA was purchased from New England Biolabs, Inc. (single-strand, N4040S). Other chemicals and solvents were purchased from Beijing Chemical Reagent Company and used without further purification. Water was purified using a Milli-Q system (Millipore, Milford, MA, U.S.A.).

Instruments

Absorbance spectra were obtained by a UV/vis spectrometer (Lambda 950, PerkinElmer Inc.). The size and morphology of BMEPC self-assembled nanoparticles were measured with a transmission electron microscope (TEM) (HT7700, Hitachi). The fluorescence

emission spectra were characterized by a fluorescence spectrometer (LS55, PerkinElmer Inc.).

Self-Assembly of Triangular-Shaped DNA Origami

Triangular-shaped DNA origami was assembled in a facile method according to the typical procedure described by Rothemund in 2006 and the method of Yan's in 2009. The long single stranded M13 scaffold and each of the unpurified short staple strands were mixed at molar ratio of 1:10. The assembly was done (10 nM) in 1× TAE (Tris-acetate-EDTA)-Mg^{2+} buffer (Tris base 40 mM; acetic acid 20 mM; EDTA 2 mM; magnesium acetate 12.5 mM; pH 8.0) by heating the mixture to 90 °C and slowly cooling to 4 °C. In order to remove the excess staple and capture strands, the assembled origami was washed 3 times with 1× TAE-Mg^{2+} buffer and passed through an Amicon filter (100kD MWCO).

BMEPC Loading on DNA Origami

BMEPC solutions (ranging from 5 to 25 μM in ddH_2O or medium) were incubated with triangular-shaped DNA origami structures (1.0 nM in ddH_2O or medium), respectively, for 12 h at room temperature in dark condition. Under these ratios, the complexes BMEPC-loaded DNA origami can be used without any further purification.

Characterizations of Unloaded and BMEPC-Loaded DNA Origami

Both DNA origami carriers and the BMEPC-loaded complexes were characterized by atomic force microscopy (AFM), UV–vis absorption and fluorescence emission spectra, and agarose gel electrophoresis (AGE). AFM imaging was done in tapping-in-buffer mode: 10 μL of sample was deposited in mica and left to adsorb to the surface for at least 10 min; subsequently, the sample was washed 3 times with ddH_2O, and then 1× TAE-Mg^{2+} buffer was added before imaging. One % AGE staining with ethidium bromide (EB) was done at room temperature. The gels were applied by a constant voltage of 80 V for 40 min in 1× TAE-Mg^{2+} buffer, and the images were collected by a gel imaging system (General Electric Co.).

Cell Culture

Human breast adenocarcinoma MCF-7 cell line was purchased from the Cell Center at the Institute of Basic Medical Sciences, Chinese Academy of Medical Science. The cells were cultured in Dulbecco's modification of Eagle's medium (DMEM) (Hyclone, Thermo Scientific) with 10% fetal bovine serum (FBS) (Hyclone, Thermo Scientific), 100 units/mL penicillin, and 100 μg/mL streptomycin (GIBICO, Invitrogen) in a 37 °C, 5% CO_2 sterile atmosphere.

Cell Viability Assay

The cytotoxicity experiments were tested using the MTT microculture assay against MCF-7 cells. Cells (2000 cells/well) were seeded on a 96-well plate in 100 μL of DMEM containing FBS and antibiotics and cultured for 24 h. The adherent cells were treated with carrier-free BMEPC or BMEPC-loaded DNA origami in DMEM, respectively. After 12 h of 37 °C incubation, the cells were washed 3 times with phosphate buffered saline (PBS, pH 7.0) at

room temperature and irradiated in DMEM without phenol red for different durations of time. Cells without irradiation were set as control. Later, the cells were cultured in 100 μL of DMEM containing FBS and antibiotics for another 72 h. The MTT assay was used to measure cell viability. Untreated cells served as the gauge for 100% viability, and media served as background.

Confocal Imaging

MCF-7 cells were cultured on glass-bottomed dishes for 24 h before observation, and the adherent cells were treated with 2 mL of DMEM containing 20 μM carrier-free BMEPC and 1.0 nM (20 μM BMEPC)-loaded DNA origami respectively for 12 h. The medium was then replaced with fresh DMEM without phenol red after the cells were washed with PBS (pH 7.0) 3 times. Finally, cells were imaged and irradiated using different confocal laser scanning microscopes (CLSM) (Carl Zeiss, PerkinElmer and Leica).

Apoptosis Fluorescence Staining

Adherent MCF-7 cells were treated with 2 mL of DMEM containing 1.0 nM (20 μM BMEPC)-loaded DNA origami for 12 h and washed with PBS (pH 7.0) for 3 times. Then the cells were irradiated using CLSM in fresh DMEM without phenol red until dead. After treated the cells were stained with Alexa Fluor 488 Annexin V/Dead Cell Apoptosis Kit (V13241, Invitrogen) according to the instruction.

ROS Staining

Adherent MCF-7 cells were treated with 2 mL of DMEM containing 20 μM carrier-free BMEPC or 1.0 nM (20 μM BMEPC)-loaded DNA origami for 12 h, and then incubated with Reactive Oxygen Species Assay Kit (CA1410, Solarbio) according to the instruction. Later, the cells were washed with PBS (pH 7.0) 3 times and irradiated using CLSM in fresh DMEM without phenol red.

Supplementary Material

Refer to Web version on PubMed Central for supplementary material.

Acknowledgments

This work was supported by the Chinese Natural Science Foundation key project (31430031) and National Distinguished Young Scholars grant (31225009), State High-Tech Development Plan (2012AA020804 and SS2014AA020708). This work was supported in part by NIH/NIMHD 8 G12 MD007597 and USAMRMC W81XWH-10-1-0767 grants. The authors also appreciate the support by the Strategic Priority Research Program of the Chinese Academy of Sciences (Grant No. XDA09030301), Beijing Natural Science Foundation (Grant No. 7152157 and 7164316), and the External Cooperation Program of BIC, Chinese Academy of Sciences (Grant No. 121D11KYSB20130006).

References

1. Lucky SS, Soo KC, Zhang Y. Nanoparticles in Photodynamic Therapy. Chem Rev. 2015; 115:1990–2042. [PubMed: 25602130]
2. Macdonald IJ, Dougherty TJ. Basic Principles of Photodynamic Therapy. J Porphyrins Phthalocyanines. 2001; 5:105–129.

3. Konan YN, Gurny R, Allémann E. State of the Art in the Delivery of Photosensitizers for Photodynamic Therapy. J Photochem Photobiol, B. 2002; 66:89–106. [PubMed: 11897509]
4. Brown SB, Brown EA, Walker I. The Present and Future Role of Photodynamic Therapy in Cancer Treatment. Lancet Oncol. 2004; 5:497–508. [PubMed: 15288239]
5. Castano AP, Demidova TN, Hamblin MR. Mechanisms in Photodynamic Therapy: Part One—Photosensitizers, Photochemistry and Cellular Localization. Photodiagn Photodyn Ther. 2004; 1:279–293.
6. Castano AP, Demidova TN, Hamblin MR. Mechanisms in Photodynamic Therapy: Part Two—Cellular Signaling, Cell Metabolism and Modes of Cell Death. Photodiagn Photodyn Ther. 2005; 2:1–23.
7. Castano AP, Demidova TN, Hamblin MR. Mechanisms in Photodynamic Therapy: Part Three—Photosensitizer Pharmacokinetics, Biodistribution, Tumor Localization and Modes of Tumor Destruction. Photodiagn Photodyn Ther. 2005; 2:91–106.
8. Oleinick NL, Morris RL, Belichenko I. The Role of Apoptosis in Response to Photodynamic Therapy: What, Where, Why, and How. Photoch Photobio Sci. 2002; 1:1–21.
9. Robertson C, Evans DH, Abrahamse H. Photodynamic Therapy (PDT): A Short Review on Cellular Mechanisms and Cancer Research Applications for PDT. J Photochem Photobiol, B. 2009; 96:1–8. [PubMed: 19406659]
10. Mroz P, Yaroslavsky A, Kharkwal GB, Hamblin MR. Cell Death Pathways in Photodynamic Therapy of Cancer. Cancers. 2011; 3:2516–2539. [PubMed: 23914299]
11. Buytaert E, Dewaele M, Agostinis P. Molecular Effectors of Multiple Cell Death Pathways Initiated by Photodynamic Therapy. Biochim Biophys Acta, Rev Cancer. 2007; 1776:86–107.
12. Yavari N, Andersson-Engels S, Segersten U, Malmstrom PU. An Overview on Preclinical and Clinical Experiences with Photodynamic Therapy for Bladder Cancer. Can J Urol. 2011; 18:5778–5786. [PubMed: 21854709]
13. Allison R, Moghissi K, Downie G, Dixon K. Photodynamic Therapy (PDT) for Lung Cancer. Photodiagn Photodyn Ther. 2011; 8:231–239.
14. Green B, Cobb AR, Hopper C. Photodynamic Therapy in the Management of Lesions of the Head and Neck. Br J Oral Max Surg. 2013; 51:283–287.
15. Kostovic K, Pastar Z, Ceovic R, Bukvic Mokos Z, Stulhofer Buzina D, Stanimirovic A. Photodynamic Therapy in Dermatology: Current Treatments and Implications. Coll Antropol. 2012; 36:1477–1481. [PubMed: 23390855]
16. Gossner L, Stolte M, Sroka R, Rick K, May A, Hahn EG, Ell C. Photodynamic Ablation of High-Grade Dysplasia and Early Cancer in Barrett's Esophagus by Means of 5-Aminolevulinic Acid. Gastroenterology. 1998; 114:448–455. [PubMed: 9496934]
17. Nguyen NT, Schauer P, Luketich JD. Minimally Invasive Esophagectomy for Barrett's Esophagus with High-Grade Dysplasia. Surgery. 2000; 127:284–290. [PubMed: 10715983]
18. Dolmans DE, Fukumura D, Jain RK. Photodynamic Therapy for Cancer. Nat Rev Cancer. 2003; 3:380–387. [PubMed: 12724736]
19. Hirschberg H, Spetalen S, Carper S, Hole P, Tillung T, Madsen S. Minimally Invasive Photodynamic Therapy (PDT) for Ablation of Experimental Rat Glioma. Minim Invasive Neurosurg: MIN. 2006; 49:135–142. [PubMed: 16921452]
20. Muragaki Y, Akimoto J, Maruyama T, Iseki H, Ikuta S, Nitta M, Maebayashi K, Saito T, Okada Y, Kaneko S, Phase II, et al. Clinical Study on Intraoperative Photodynamic Therapy with Talaporfin Sodium and Semiconductor Laser in Patients with Malignant Brain Tumors: Clinical Article. J Neurosurg. 2013; 119:845–852. [PubMed: 23952800]
21. Rigual NR, Shafirstein G, Frustino J, Seshadri M, Cooper M, Wilding G, Sullivan MA, Henderson B. Adjuvant Intraoperative Photodynamic Therapy in Head and Neck Cancer. JAMA Otolaryngol Head Neck Surg. 2013; 139:706–711. [PubMed: 23868427]
22. Akimoto J, Haraoka J, Aizawa K. Preliminary Clinical Report on Safety and Efficacy of Photodynamic Therapy Using Talaporfin Sodium for Malignant Gliomas. Photodiagn Photodyn Ther. 2012; 9:91–99.
23. Sun Y, Joyce LE, Dickson NM, Turro C. Efficient DNA Photocleavage by [Ru (Bpy) 2 (Dppn)] 2+ with Visible Light. Chem Commun. 2010; 46:2426–2428.

24. Zhou C, Liu Q, Xu W, Wang C, Fang X. A Water-Soluble C 60-Porphyrin Compound for Highly Efficient DNA Photocleavage. Chem Commun. 2011; 47:2982–2984.
25. Singh V, Mondal PC, Kumar A, Jeyachandran YL, Awasthi SK, Gupta RD, Zharnikov M. Surface Confined Heteroleptic Copper (II)—Polypyridyl Complexes for Photonuclease Activity. Chem Commun. 2014; 50:11484–11487.
26. Zhou Q-X, Lei W-H, Li C, Hou Y-J, Wang X-S, Zhang B-W. DNA Photocleavage in Anaerobic Conditions by a Ru (II) Polypyridyl Complex with Long Wavelength MLCT Absorption. New J Chem. 2010; 34:137–140.
27. Karwa AS, Poreddy AR, Asmelash B, Lin T-S, Dorshow RB, Rajagopalan R. Type 1 Phototherapeutic Agents, Part I: Preparation and Cancer Cell Viability Studies of Novel Photolabile Sulfenamides. ACS Med Chem Lett. 2011; 2:828–833. [PubMed: 24900271]
28. Ogawa K, Kobuke Y. Anti-Cancer Agents Med Chem. 2008; 8:269.
29. Zheng Q, Jockusch S, Zhou Z, Blanchard SC. The Contribution of Reactive Oxygen Species to the Photobleaching of Organic Fluorophores. Photochem Photobiol. 2014; 90:448–454. [PubMed: 24188468]
30. Zheng Y-C, Zheng M-L, Li K, Chen S, Zhao Z-S, Wang X-S, Duan X-M. Novel Carbazole-Based Two-Photon Photosensitizer for Efficient DNA Photocleavage in Anaerobic Condition Using Near-Infrared Light. RSC Adv. 2015; 5:770–774.
31. Krammer B. Vascular Effects of Photodynamic Therapy. Anticancer Res. 2001; 21:4271–4277. [PubMed: 11908681]
32. Sun Y, Joyce LE, Dickson NM, Turro C. DNA Photocleavage by an Osmium(II) Complex in the PDT Window. Chem Commun. 2010; 46:6759–6761.
33. Frangioni JV. *In Vivo* Near-Infrared Fluorescence Imaging. Curr Opin Chem Biol. 2003; 7:626–634. [PubMed: 14580568]
34. Mei Q, Wei X, Su F, Liu Y, Youngbull C, Johnson R, Lindsay S, Yan H, Meldrum D. Stability of DNA Origami Nanoarrays in Cell Lysate. Nano Lett. 2011; 11:1477–1482. [PubMed: 21366226]
35. Schüller VJ, Heidegger S, Sandholzer N, Nickels PC, Suhartha NA, Endres S, Bourquin C, Liedl T. Cellular Immunostimulation by CpG-Sequence-Coated DNA Origami Structures. ACS Nano. 2011; 5:9696–9702. [PubMed: 22092186]
36. Douglas SM, Bachelet I, Church GM. A Logic-Gated Nanorobot for Targeted Transport of Molecular Payloads. Science. 2012; 335:831–834. [PubMed: 22344439]
37. Li J, Pei H, Zhu B, Liang L, Wei M, He Y, Chen N, Li D, Huang Q, Fan C. Self-Assembled Multivalent DNA Nanostructures for Noninvasive Intracellular Delivery of Immunostimulatory CpG Oligonucleotides. ACS Nano. 2011; 5:8783–8789. [PubMed: 21988181]
38. Jiang Q, Song C, Nangreave J, Liu X, Lin L, Qiu D, Wang Z-G, Zou G, Liang X-J, Yan H, et al. DNA Origami as a Carrier for Circumvention of Drug Resistance. J Am Chem Soc. 2012; 134:13396–13403. [PubMed: 22803823]
39. Rothemund PW. Folding DNA to Create Nanoscale Shapes and Patterns. Nature. 2006; 440:297–302. [PubMed: 16541064]
40. Dumat B, Bordeau G, Faurel-Paul E, Mahuteau-Betzer F, Saettel N, Bombled M, Metge G, Charra F, Fiorini-Debuisschert C, Teulade-Fichou MP. N-Phenyl-Carbazole-Based Two-Photon Fluorescent Probes: Strong Sequence Dependence of the Duplex *Vs* Quadruplex Selectivity. Biochimie. 2011; 93:1209–1218. [PubMed: 21672604]
41. Chhabra R, Sharma J, Ke Y, Liu Y, Rinker S, Lindsay S, Yan H. Spatially Addressable Multiprotein Nanoarrays Templated by Aptamer-Tagged DNA Nanoarchitectures. J Am Chem Soc. 2007; 129:10304–10305. [PubMed: 17676841]
42. Tørring T, Voigt NV, Nangreave J, Yan H, Gothelf KV. DNA Origami: A Quantum Leap for Self-Assembly of Complex Structures. Chem Soc Rev. 2011; 40:5636–5646. [PubMed: 21594298]
43. Nangreave J, Han D, Liu Y, Yan H. DNA Origami: A History and Current Perspective. Curr Opin Chem Biol. 2010; 14:608–615. [PubMed: 20643573]

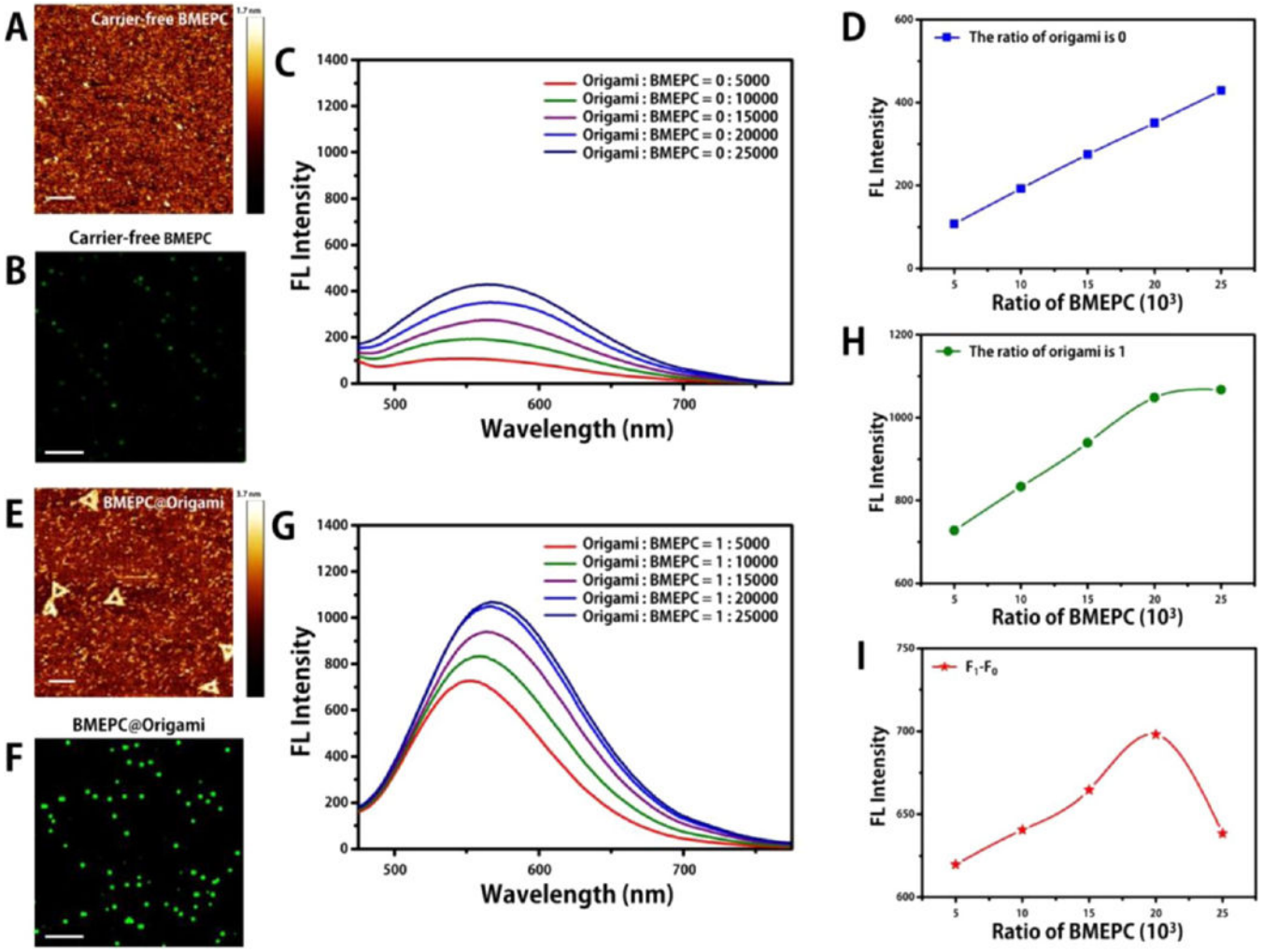

Figure 1.

Carrier-free BMEPC (A, B, C, D). (A) AFM image of carrier-free BMEPC in ddH_2O, the scale bar is 200 nm. (B) CLSM image of carrier-free BMEPC in ddH_2O, the scale bar is 2 μm. (C) Fluorescence spectra of carrier-free BMEPC in ddH_2O. (D) Fluorescence emission of the maximum peak intensity corresponding to different BMEPC ratios in carrier-free BMEPC. BMEPC-loaded DNA origami (E, F, G, H). (E) AFM image of BMEPC-loaded DNA origami in ddH_2O, the scale bar is 200 nm. (F) CLSM image of BMEPC-loaded DNA origami in ddH_2O, the scale bar is 2 μm. (G) Fluorescence spectra of BMEPC-loaded DNA origami of different BMEPC molar ratios in ddH_2O. (H) Fluorescence emission of the maximum peak intensity corresponding to different BMEPC ratios in BMEPC-loaded DNA origami. (I) Difference of fluorescence emission between BMEPC-loaded DNA origami and carrier-free BMEPC under the same ratio of BMEPC molecules, using the corresponding points in (H) minus those in (D).

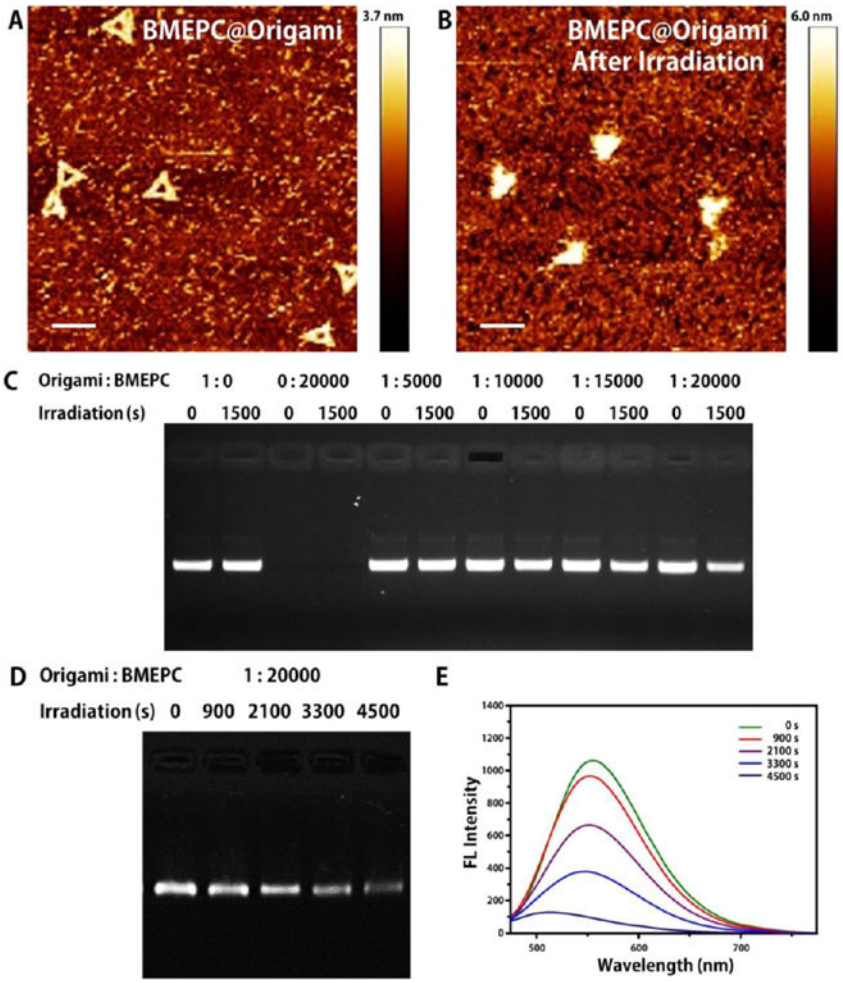

Figure 2.

(A) AFM image of BMEPC-loaded DNA origami complex before irradiation. (B) AFM image of BMEPC-loaded DNA origami complex after irradiation. (C) AGE patterns of the photocleaved triangular-shaped DNA origami influencing corresponding to different BMEPC ratios. (D) AGE patterns of the photocleaved BMEPC-loaded DNA origami influencing corresponding to different durations of irradiation time. (E) One-photon induced fluorescence emission spectra of BMEPC-loaded DNA origami complex after different durations of irradiation time at 405 nm. (Lamp: 365 nm, 8 W. Optical Density: 0.067 W/cm^2. Irradiation distance: 1 cm.)

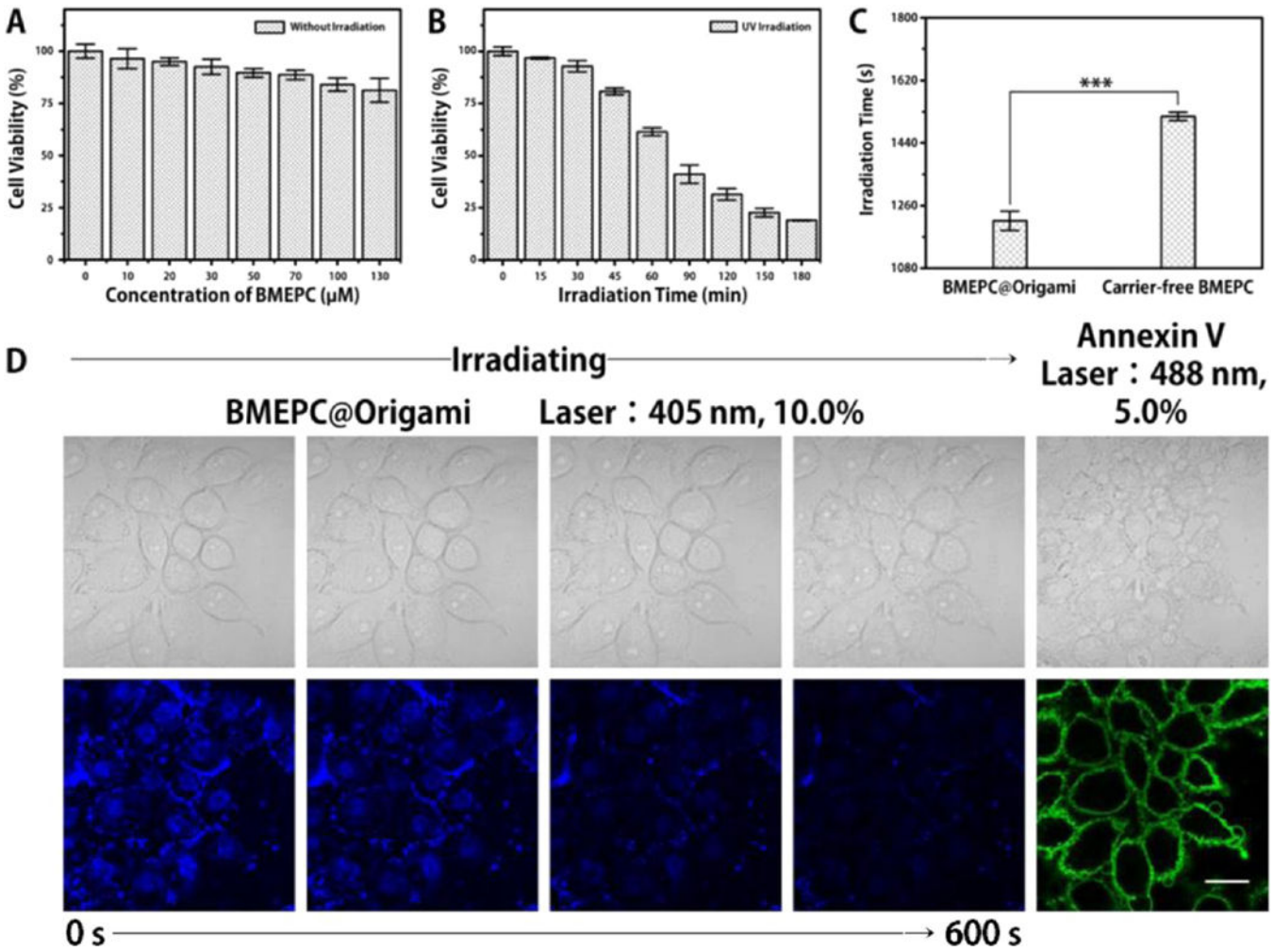

Figure 3.

(A) Cell viability of MCF-7 cells after incubated with different concentrations of BMEPC for 12 h in darkness. (B) Cell viability of MCF-7 cells after irradiated in DMEM (phenol red free) for different durations of time. (C) Time to 50% inhibition of irradiation after incubation with 20 μM carrier-free BMEPC and 1 nM (20 μM BMEPC-loaded) DNA origami complex individually for 12 h, and then irradiated in DMEM (phenol red free), p = 0.0002. (Lamp: 365 nm, 8 W. Optical Density: 0.067 W/cm^2. Irradiation distance: 1 cm.) (D) One-photon induced CLSM irradiation (blue) and Annexin V apoptosis fluorescence staining (green) at 405 nm. Adhered MCF-7 cells were incubated with 1 nM (20 μM BMEPC-loaded) DNA origami for 12 h in DMEM, irradiating in DMEM (phenol red free) for 600 s and imaging in Annexin V binding buffer. The scale bars are 25 μm.

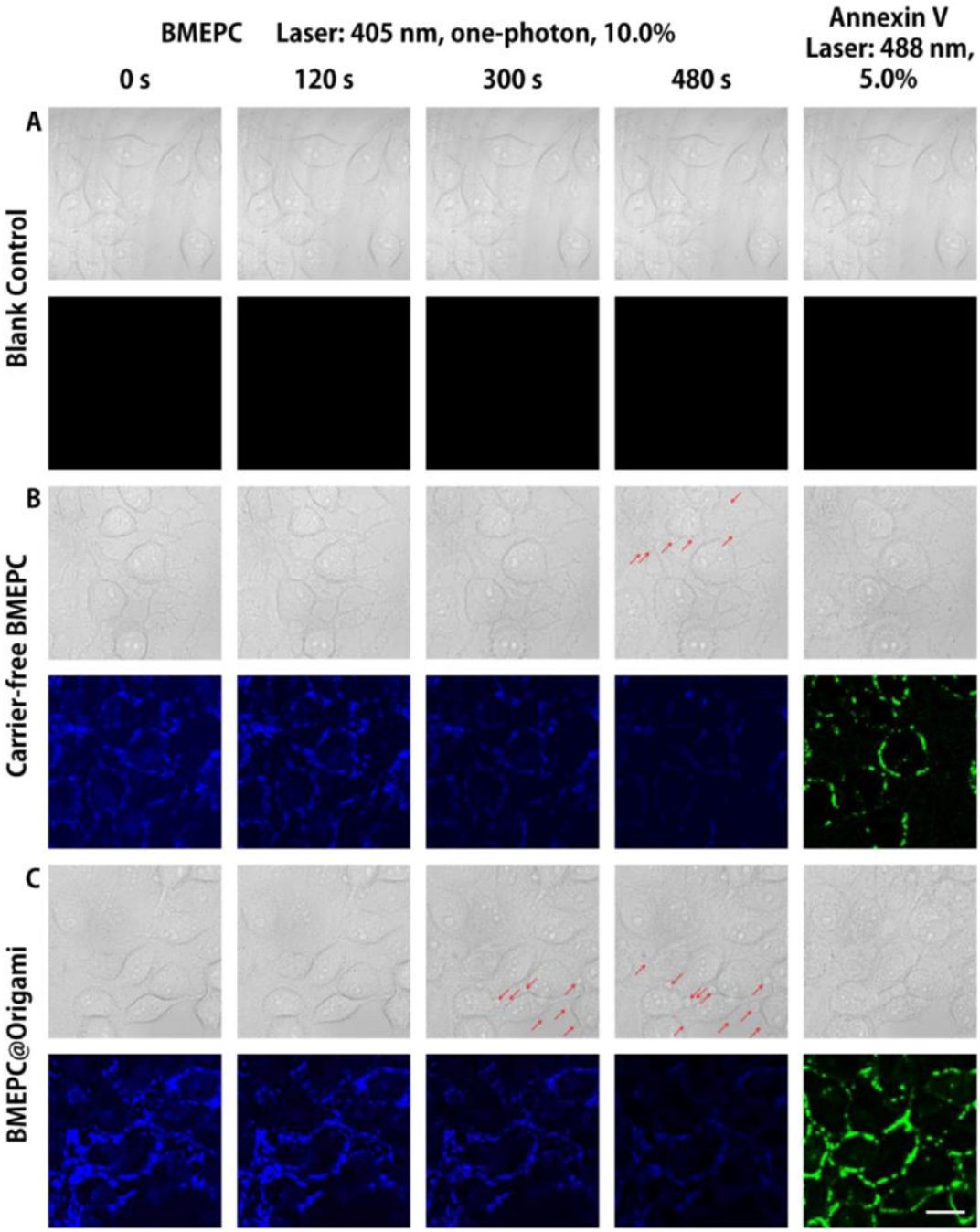

Figure 4.

One-photon induced CLSM imaging and irradiating at 440 nm. Adhered MCF-7 cells (A) were incubated with 20 μM carrier-free BMEPC (B) and 1 nM (20 μM BMEPC-loaded) DNA origami complex (C) individually for 12 h in DMEM and then irradiated for 480 s in DMEM (phenol red free). The scale bar is 25 μm.

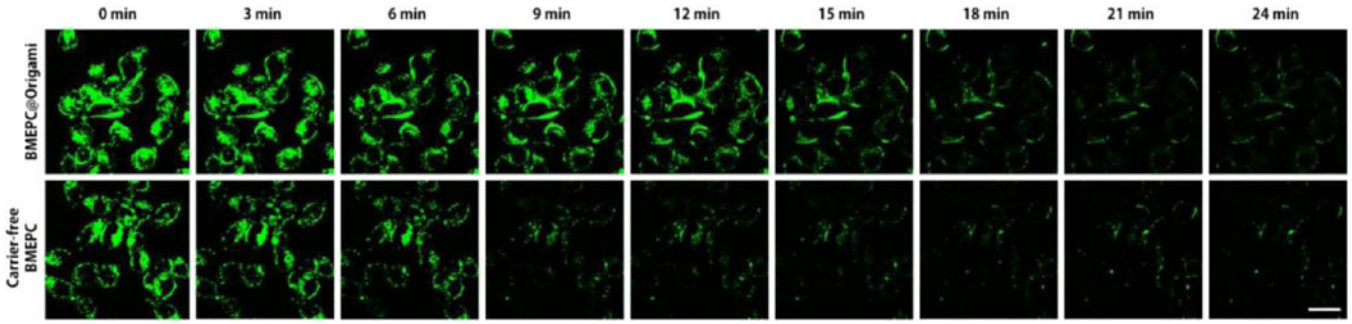

Figure 5.

One-photon induced CLSM imaging at 405 nm. Adhered MCF-7 cells were incubated with 1.0 nM (20 μM BMEPC-loaded) DNA origami and 20 μM carrier-free BMEPC, respectively, for 12 h in DMEM and imaging in DMEM (phenol red free). The scale bar is 25 μm.

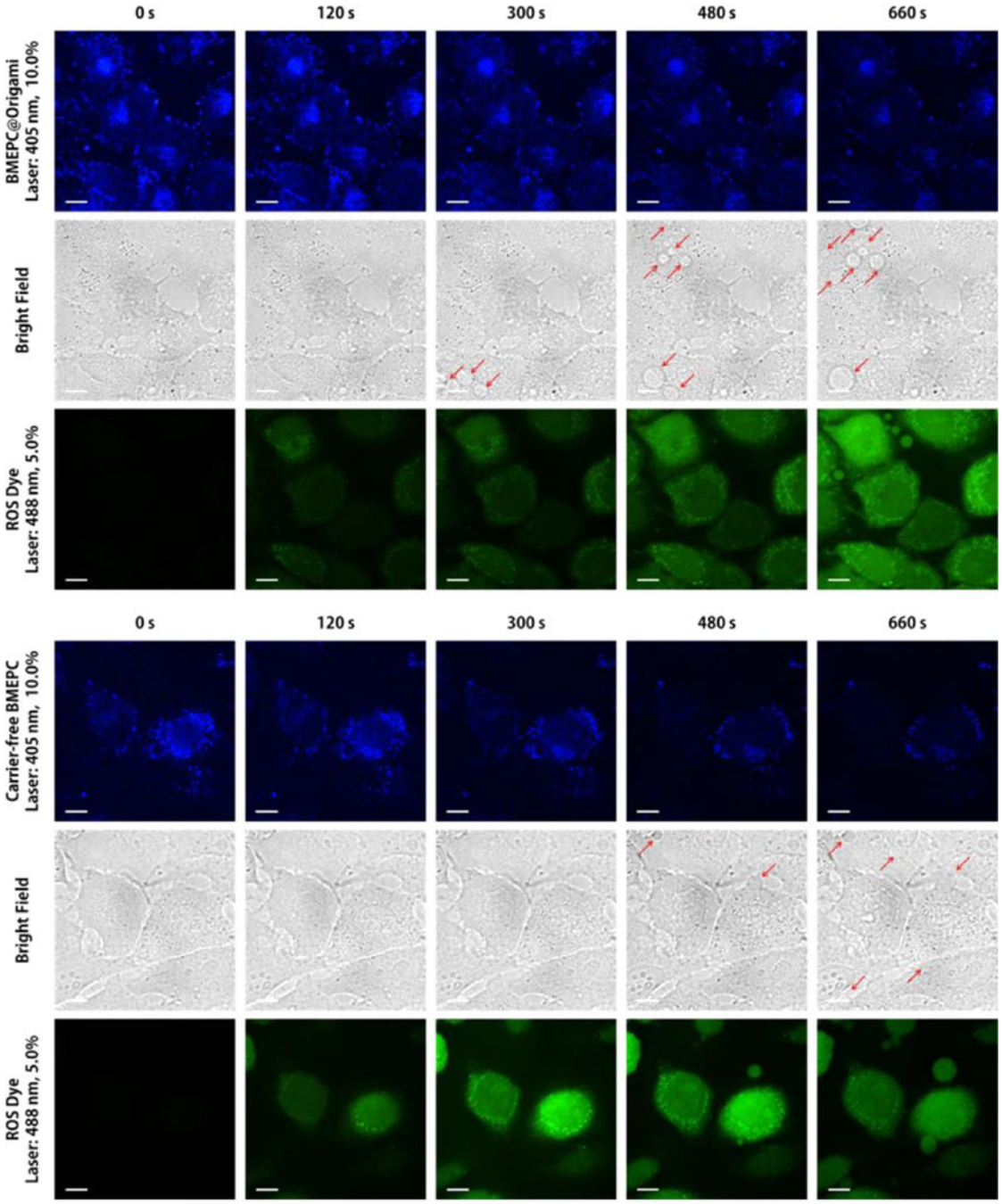

Figure 6.

One-photon induced apoptosis staining at 440 nm. Adhered MCF-7 cells were incubated with either 20 μM carrier-free BMEPC or 1 nM (20 μM BMEPC-loaded) DNA origami complex for 12 h in DMEM and then incubated with DCFH-DA for 30 min. Later, the cells were irradiated for 660 s in DMEM (phenol red free). The scale bars are 10 μm.

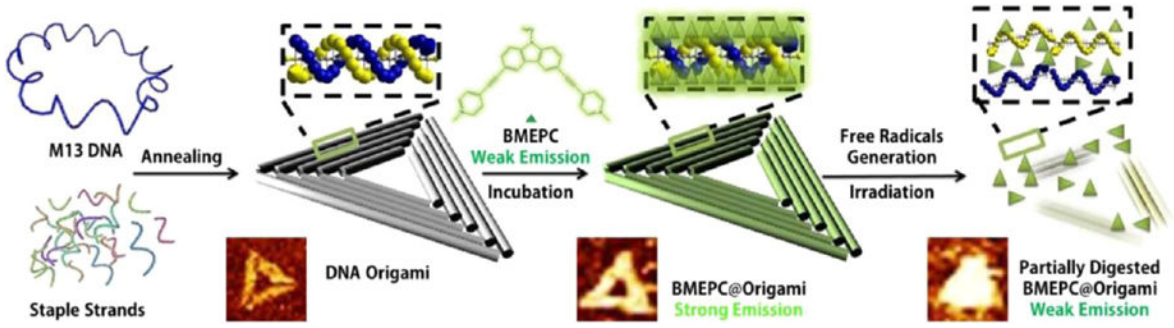

Scheme 1.

Schematic Representation Showing the Preparation of Triangular-Shaped DNA Origami and BMEPC-Loaded DNA Origami Complex Assembling and Functioning